JMEPEG (2023) 32:5566–5575
https://doi.org/10.1007/s11665-022-07504-x

1059-9495/$19.00

TECHNICAL ARTICLE

The Effect of TiN-TiB_2 on the Microstructure, Wear, and Nanoindentation Behavior of Ti6Al4V-Ni-Cr Matrix Composites

Oluwasegun Eso Falodun, Samuel Ranti Oke, Samuel Olukayode Akinwamide, Olawale Olarewaju Ajibola, Abdullahi Olawale Adebayo, Sunday Gbenga Borisade, Adeolu Adesoji Adediran, and Peter Apata Olubambi

Submitted: 17 June 2022 / Revised: 12 September 2022 / Accepted: 23 September 2022 / Published online: 13 October 2022

The influence of ceramic (TiN and TiB_2) particles on the densification, microstructure, wear, and nanoindentation behavior of titanium matrix composites produced by spark plasma sintering was investigated. The results showed that the relative density of the Ti6Al4V-Ni-Cr-matrix composite with TiN and TiB_2 was reduced from 99.51 to 95.33%. The microstructural analysis revealed that the reinforcements were dispersed uniformly within the composite, demonstrating the existence of lamellar (α and β phase) and bimodal structures. The average microhardness value gradually increased from 378 to 707 $HV_{0.2}$, while the coefficient of friction ranged between 0.3 and 0.65. Furthermore, the material resisted the wear mechanism with improved wear resistance. The decreased frictional coefficient exhibited by the reinforced composite might be attributed to the oxide-layer formation, which served as a lubricant reducing friction between the two gliding surfaces of the material. The nanohardness values ranged from 6363.3 to 10,343 MPa, while the reduced-elastic-modulus values varied from 122.9 to 158.93 GPa.

Keywords ceramic particles, microstructure, nanoindentation behavior, spark plasma sintering, titanium alloys

1. Introduction

Titanium and titanium alloys are essential because of their unique properties: high strength-to-weight ratio, low density, and superior corrosion resistance. They are widely used in the aerospace, biomedical, and automotive industries. Despite the limitations of titanium and titanium alloys, the development of titanium-based composites has provided several advantages through the combination of physical and mechanical properties. This makes titanium and titanium alloys suitable for a wide range of applications. The use of ceramic reinforcement improves the mechanical and tribological properties of these materials. Powder metallurgy processes mainly produce titanium matrix composites (TMCs) due to their simplicity and production techniques. However, powder metallurgy almost entirely facilitates the manufacture of materials and controls the determination of the final properties of titanium matrix composites (Ref 1). The most common method for ensuring that the material has better mechanical properties is controlling the matrix/secondary phase interfaces (Ref 2). Powder metallurgy overcomes older technology's shortcomings, such as reinforcement phase contamination, wettability between the matrix and ceramic additives, and prolonged processing stages.

Much effort has been made in synthesizing alloys or ceramic reinforcement to enhance the mechanical characteristics of titanium composites. The process of strengthening titanium alloys with ceramic materials, by means of a spark plasma sintering technique, is a current research focus in the area of the strengthening of the mechanical properties of titanium and its alloys. The introduction of TiN reduced grain growth by enhancing densification and mechanical properties of titanium and its alloys (Ref 3). Purwar et al. (Ref 4) investigated the effect of Ti addition on the mechanical properties and sinterability of ZrB_2-based ceramic composites. They reported that adding Ti to ZrB_2 18 wt.% SiC-based composites improved densification while increasing hardness (up to 29 GPa) and indentation toughness (up to 9 $MPa{\cdot}m^{1/2}$). Namini et al. (Ref 2) studied the effect of TiB_2 reinforcement on titanium-based composites, using the spark plasma sintering technique. The addition of 9.6 wt.% TiB_2 resulted in a nearly dense sample (99.6%). However, the x-ray diffraction analysis and microstructural characterization confirmed the in situ synthesis

Oluwasegun Eso Falodun, Department of Mechanical Engineering, Covenant University, Ota, Ogun State, Nigeria; and Centre for Nanomechanics and Tribocorrosion, University of Johannesburg, Johannesburg, Gauteng, South Africa; **Samuel Ranti Oke**, Centre for Nanomechanics and Tribocorrosion, University of Johannesburg, Johannesburg, Gauteng, South Africa; and Department of Metallurgical and Materials Engineering, Federal University of Technology, Akure, Ondo State, Nigeria; **Samuel Olukayode Akinwamide**, Advanced Manufacturing and Materials Research Group, Department of Mechanical Engineering, Aalto University, Espoo, Finland; **Olawale Olarewaju Ajibola, Abdullahi Olawale Adebayo,** and **Sunday Gbenga Borisade**, Department of Materials and Metallurgical Engineering, Federal University Oye Ekiti, Oye-Ekiti, Nigeria; **Adeolu Adesoji Adediran**, Department of Mechanical Engineering, Landmark University, Omu-Aran, Kwara State, Nigeria; and **Peter Apata Olubambi**, Centre for Nanomechanics and Tribocorrosion, University of Johannesburg, Johannesburg, Gauteng, South Africa. Contact e-mails: segzy201@gmail.com and oluwasegun.falodun@covenantuniversity.edu.ng.

Table 1 Elemental powder composition of sintered titanium matrix composite

Ti6Al4V, vol.%	Cr, vol.%	Ni, vol.%	TiN, vol.%	TiB_2, vol.%
100	...	...	...	...
95	5	...	...	...
90	5	5	...	...
88	5	5	2	...
85	5	5	5	...
88	5	5	...	2
85	5	5	...	5

of TiB_2 in sintered samples, and the increase in the tensile strength of the composite samples as TiB_2 content rose to 4.8 wt.%.

However, adding ceramic particles usually results in a significant ductility degradation of the metal matrix composites (Ref 5). The introduction of beta-stabilizing elements (β-eutectoid), such as nickel and chromium, aims to restore some ductility and strength to the titanium-based composite and enhance the amount of β phase in the matrix, through the addition of ceramic. The β phase of titanium and titanium alloys is also more ductile than the α phase, with the ductility of the β phase being essentially unaffected by the degree of interstitial (Ref 6, 7). The mechanical properties of titanium diboride (TiB_2), such as high stiffness, high Young's modulus, high strength-to-weight ratio, excellent chemical and thermal stability, have attracted interest in various applications (Ref 8, 9). Titanium nitride has a single FCC structure, a good chemical and thermal compatibility, more stability at higher temperatures, and sufficient diffusion at the interface. This ensures efficient bonding and strength, as well as extraordinarily high hardness and creep resistance (Ref 10, 11). This makes it an excellent reinforced phase with good wettability in the metal matrix.

Spark plasma sintering (SPS) is an innovative, environmentally friendly, fast-sintering technology that may quickly densify sintered powder, reduce grain growth, and sinter at a lower temperature (Ref 12, 13). Spark plasma sintering is a rapid application that combines plasma generation with resistive heat and pressure, to allow particle composites to compact entirely and near their maximum intense theoretical density, even at low temperatures and in a short period (Ref 14). Unlike conventional sintering processes such as hot pressing, hot isostatic pressing, and microwave sintering, spark plasma sintering permits the complete densification of powder composites and near-full theoretical densities at less sintering time and lower temperature. These factors illustrate diverse sintering techniques suitable for consolidating a wide range of powders (Ref 15-18). During spark plasma sintering, an excessive pulsed electric current is applied to the electrodes, a plasma is frequently generated between the powder particles, and the microscopic electric voltage is then released in the voids between the powder particles, causing material exchange at a rapid distribution rate, and the generation of a plasma. This turns the powder into a coherent mass, without melting (Ref 19-21). Because solidification occurs fast, spark plasma sintering provides a method for modifying the microstructure, and thus promoting grain-size retention while minimizing undesirable grain-growth effects. The advantage of a short processing time is that it assists in reaching the required grain size, enhancing the final output's mechanical properties (Ref 22). Therefore, spark plasma sintering may be an excellent method for producing high-density refractories and metals with fine microstructure.

As a non-destructive testing technique, nanoindentation has recently been employed as an in situ indentation-measuring method to determine the mechanical properties of materials, including metals, ceramics, polymers, and composites, with a wide range of geometries and without altering the materials' microstructural orientation or causing significant damage (Ref 23, 24). Maja et al. (Ref 11) examined the mechanical characteristics of titanium alloy and titanium-reinforced titanium nitride, using the load-displacement curve formed during nanoindentation to determine the elastic modulus and nanohardness. They observed that using a nanosized titanium nitride enhanced the nanohardness of Ti6Al4V from 5329 to 7517 MPa, while the average elastic modulus increased from 139 to 156 GPa. Moreover, Okoro et al. (Ref 25) studied the nanoindentation behavior of sintered multiwall carbon-nanotubes-reinforced-titanium alloys. It was observed that nanohardness and reduced elastic modulus had increased from 4677 to 9276 MPa and from 29.3 to 60.9 GPa, respectively. The nanoindentation was used to evaluate the mechanical characteristics of Ti-based materials with Fe and Ta additions. The alloy's hardness and elastic recovery were also in the 3.38-5.73 GPa and 0.241-0.298 ranges, respectively (Ref 26).

The current research aims to restore and enhance certain ductility levels and strength properties of titanium matrix composites by incorporating nickel and chromium elements. The inclusion of ceramic particles affects the characteristics of the materials. Chromium is required to activate the material precipitation activity at grain boundaries and to reduce the possibility of grain-boundary slides (Ref 27, 28), while nickel is an outstanding solid solution-strengthening agent. In this study, the spark plasma sintering approach was used to examine the influence of Ti6Al4V-Ni-Cr matrix with ceramic (TiN and TiB_2) addition on the densification, microstructure evolution, phase analysis, hardness, wear, and nanoindentation behavior of titanium composites.

2. Experimental Procedure

2.1 Material Processing of the Sintered Titanium Matrix Composites

The primary elemental powders used in the titanium matrix composites were Ti6Al4V (99.9% purity), nickel (99.5% purity), and chromium (99.9% purity). Titanium nitride (97% purity) and titanium diboride (99.9% purity) served as reinforcing phases. The powder was blended for 10 h at 150 rpm, using an effective milling procedure with a ball-to-powder ratio of 10:1 utilizing 5 mm alumina balls (Retch PM 100) in dry form. The composite powder was compacted into a 20 mm die with a 10 kN load in cylindrical graphite die, to attain green strength before sintering. Spark plasma sintering (HHPD-25, model FCT GmbH, Germany) was utilized for consolidation under vacuum at 1100 °C, with a dwell duration of 5 min, a heating rate of 100 °C/min, and a pressure of 50 MPa.

2.2 Material Characterization and Nanoindentation of Sintered Titanium Matrix Composites

Titanium matrix sintered materials were grinded with silicon carbide paper and polished with diamond suspension and colloidal silica suspension, to achieve a mirror-like surface. The densities were measured using distilled water as the immersion medium, following Archimedes' principle. The sintered samples were cut using a precision machine, and their cross sections were mounted, ground, polished, and etched with Kroll's reagents, to reveal the microstructure's features. The microstructure was studied using a scanning electron microscope (JEOL Model JSM-7600F) with energy-dispersive x-ray spectroscopy (EDS). The x-ray diffraction on the sintered composites was studied using a Philips diffractometer (PANalytical Empyrean PW1710) with monochromatic Cu Kα radiation at 40 kV and 40 mA, to determine the constituent phases.

The microhardness values of the samples were obtained using a Vickers tester (FALCON 500 series) with a load of 100 gf and a dwell time of 15 s. The ball-on-disk tribometer technique was used to examine the wear behavior of titanium-based composites. The tests were performed in dry conditions, at room temperature, using a stainless-steel ball with a diameter of 6 mm, a rotation speed of 300 rpm, a sliding time of 1800s, and a force of 10 N. The nanomechanical properties of the synthesized titanium-based composites were tested at room temperature, using a CSM Nanoindentation tester following ISO 14577. The Berkovich diamond indenter, a three-sided pyramid, was attached to the nanoindentation tester. The nanoindentation equipment was calibrated using a fused silica reference sample, to ensure that the experimental findings remained valid and accurate. The nanoindentation test was performed at a loading and unloading rate of 20 mN/min, with a maximum load of 5 mN. This study used a 15-s pause and more than 15 indentations on each piece, to avoid the viscoelastic effect and measure the time-dependent deformation of the samples. Oliver and Pharr's approach was used to determine such nanomechanical properties as nanohardness, reduced elastic modulus, and elastic-plastic behavior.

3. Results and Discussion

3.1 Densification Behavior

The effect of sintering temperature, displacement, and shrinkage rate on a sintered titanium matrix composite, as a function of sintering time, is presented in Fig. 1a-c. The initial sintering temperature was kept constant at 250 °C for 450-600 s, and the sintering temperature was raised to 1100 °C for 10 min, leading to different grain-growth rates. Figure 1b depicts the relative displacements of the punches as a sintering-time function. At the initiation of the sintering process, at around 250 °C, the relative displacement increased from 0 to 0.41 mm. The particle rearrangement occurred between 0.5 and 3.5 mm for the reinforced composite and between 1 and 3 mm for the Ti6Al4V alloy. When the sintering temperature rose from 250 to 1100 °C, the powder particles were displaced, incorporating air and trapped gases into the composite.

The increased displacement may be due to the use of reinforcements that limit the rearrangement caused by the presence of ceramic particles during compaction. This shows how the physical state and structure of the powder change during the various sintering stages (Ref 29). During sintering, the punch progression correlates to a relative displacement of 2.8-4 mm in the titanium matrix composite's cooling cycle. This significant movement of the energy during the cooling process can be explained by the composites' shrinkage, compaction, and necking. Figure 1c depicts the shrinkage rate of a sintered titanium matrix composite during spark plasma sintering, against the total sintering time. However, the shrinkage behavior of all sintered materials demonstrates three stages of shrinkage. The initial peak illustrates the rearranging of the powder particles, the removal of trapped gases, and the introduction of sparks and reinforcement particles into the matrix. This is due to the applied pressure and driving force created by the upper and lower punches (Ref 30). This first peak primarily applies to Ti6Al4V, with little rearrangement in other sintered materials. The rise in the second shrinkage peak, from 600 to 1200 s, is due to the Joule heating of the powder particle boundaries' local plastic deformation. The Joule heating cycle often occurs at high sintering temperatures, promoting atomic diffusion, melting, assembly, necking formation at the interface region, and plastic movement within the powder particles. The third peak exhibits a shrinkage reduction between 1200 and 1800s. By lowering the sintering temperature and cooling the sintering medium, the pores in the sinter close, and a solidification path arrangement is obtained.

Figure 2 shows the relative density of the sintered composite samples. Adding 5, 10, 15, and 20% TiB_2 decreased the relative density from 99.51% to 95.33%. This might be explained by increased porosity, sintering temperature and time when reinforcement is introduced, resulting in decreased material density (Ref 31, 32**)**. This phenomenon explains the

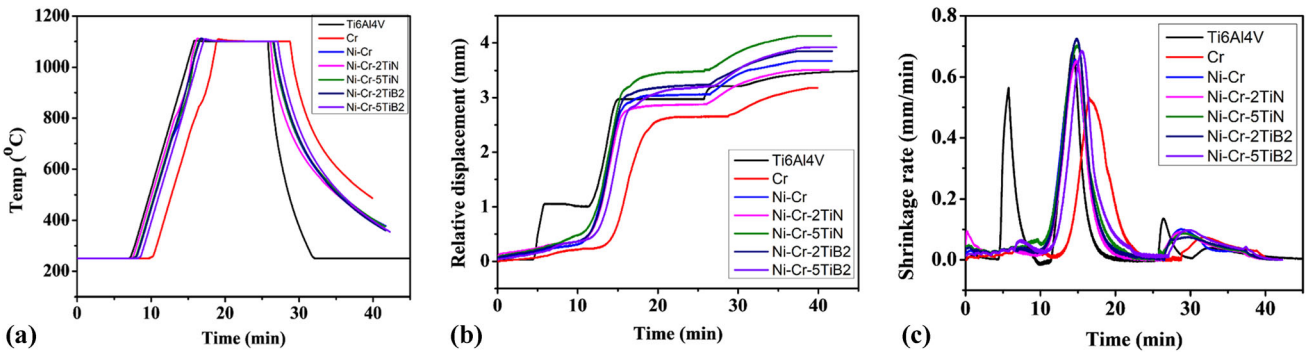

Fig. 1 The sintering process of a spark plasma against time: **a** sintering temperature, **b** relative displacement, and **c** shrinkage rate

presence of the ceramic addition phase and its reactivity with titanium alloys. This further impedes the diffusion process during sintering, decreasing the final relative density (Ref 33). However, increasing the reinforcement addition might be detrimental to density reduction (Ref 34).

3.2 Microstructural and x-ray Diffraction Analyses

The scanning electron micrographs of sintered titanium matrix composites are shown in Fig. 3. These titanium matrix composites were sintered at a temperature of 1100 °C, higher than the allotropic transition of 882 °C. This promotes the transformation of α-Ti to β-Ti during sintering. Nevertheless, the transformation process was incomplete because of the high cooling rate, which resulted in some retained β phases at α-Ti grain boundaries. Figure 3a shows the microstructure of Ti6Al4V alloy, which comprises two phases: the alpha (α) phase appearing as light gray platelets and the beta phase appearing as dark gray plates between the alpha platelets. Figure 3b, c depicts the titanium-based composite with chromium and nickel additions. The micrographs indicate chromium and nickel particles diffused into the Ti6Al4V matrix along the grain boundaries during sintering. These transformations involve the α phase nucleation at the β grain boundary, leading to the formation of intergranular β and α structures in the grain. Figure 4a, b indicates the presence of in situ TiB whiskers in the composite samples.

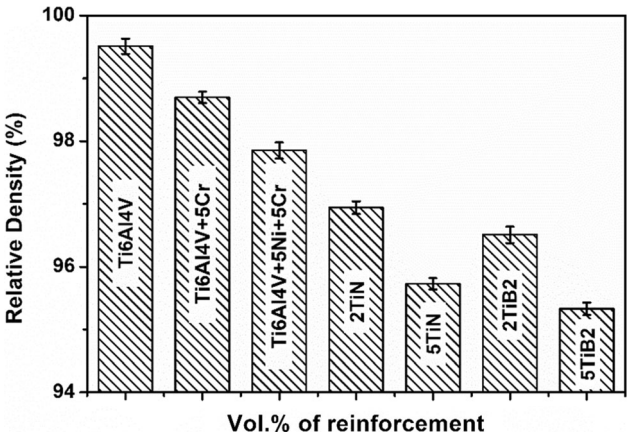

Fig. 2 Relative density of the sintered titanium matrix composite

The residual TiB_2 phase is visible in the micrographs, confirming the incomplete interaction process of TiB_2 with the matrix powder. This could be due to the high melting temperature of the reinforcement, and the increasing percentage of particles with the shortest holding time (Ref 35). The orthorhombic crystal structure of TiB and its one-dimensional development along the [010] direction initiate the production of whisker-like morphology (Ref 36). Figure 4c, d shows a bimodal microstructure, and a distinct pattern in the matrix indicates a bimodal TiN ceramic dispersion (Ref 37, 38). The addition of TiN causes the nucleation and formation of β-Ti, which aids in the α to β transformation process. The β-Ti created at high sintering temperatures was maintained at ambient temperature due to the rapid cooling of the spark plasma sintering process. Esmaily et al. (Ref 39) stated that the cooling rate considerably influences the microstructure and mechanical parameters.

The XRD diffractographs of sintered Ti6Al4V-Ni-Cr with TiN-TiB_2 addition are shown in Fig. 5. The diffraction peaks demonstrate the existence of (α and β-Ti) phases. However, nickel and chromium, which act as stabilizers of the titanium matrix β-phase, helped to generate the peaks.

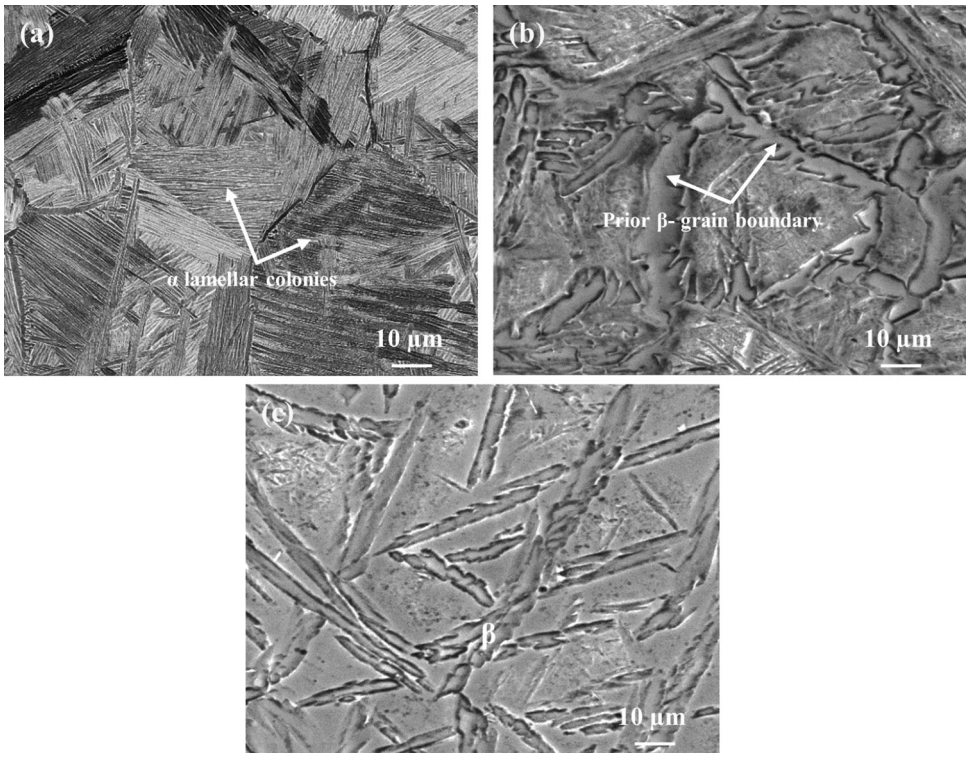

Fig. 3 SEM micrographs of sintered titanium matrix composite **a** Ti6Al4V, **b** Ti6Al4V-Cr, and **c** Ti6Al4V-Cr-Ni

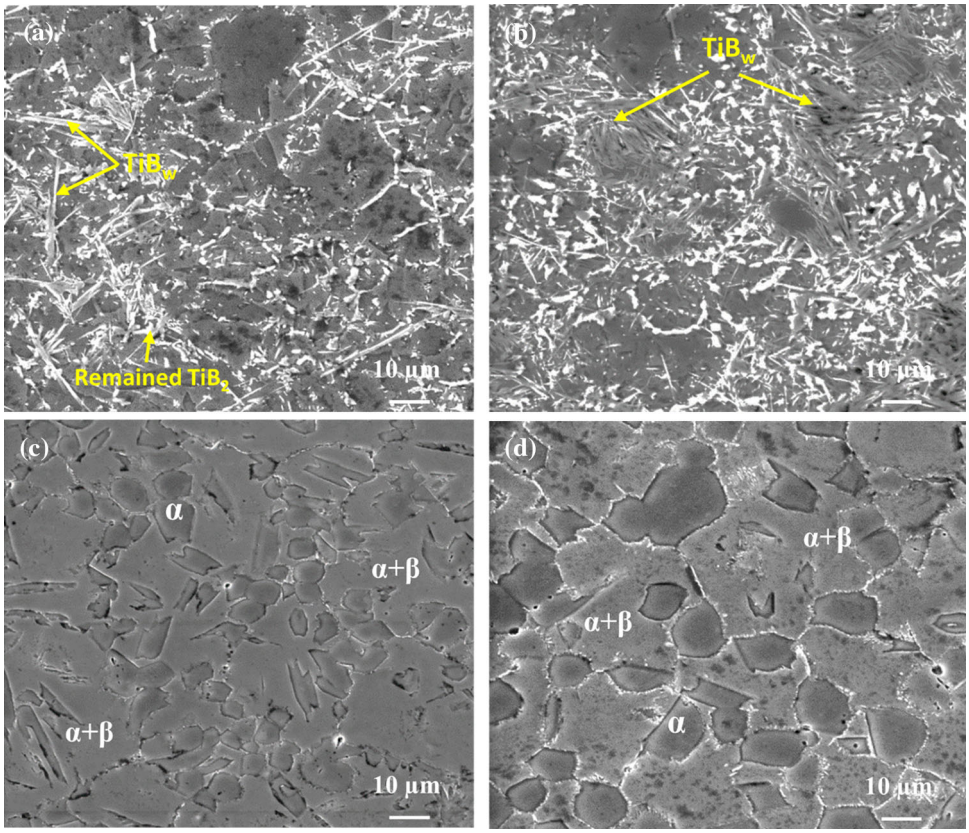

Fig. 4 SEM micrographs of sintered titanium matrix composite **a** Ti6Al4V-Cr-Ni-2TiB_2, **b** Ti6Al4V-Cr-Ni-5TiB_2, **c** Ti6Al4V-Cr-Ni-2TiN, and **d** Ti6Al4V-Cr-Ni-5TiN

Thus, adding ceramic additives resulted in a slight decrease in the intensity of α and β peaks in Fig. 5a. This decrease in peak intensity may be related to the x-ray absorption effect; however, including other elements in the Ti6Al4V matrix, the intensity of the diffraction peak shifts to higher angles in the entire composites, because of the high tensile stress of the α phase (Ref 40). The addition of 5 vol.% TiB_2 showed that the intensity of the diffraction peaks was increased and broadened, compared to 2 vol.% TiB_2. It is important to note that the secondary forming phases are refractory, which will improve the properties of the ceramic composite materials developed. Figure 5 confirms the presence of the α-Ti phase at the diffraction angles 2θ = 35.43°, 38.38°, 40.47°, 53.23°, 63.62°, and 76.81; while other peaks are 28.58°, 39.76°, 67.01°, and 72.17°. The Ti6Al4V matrix dominated the peaks. Nonetheless, adding TiN and TiB_2 decreases the peaks of the α-Ti phase at diffraction angles.

3.3 Hardness of Sintered Titanium Matrix Composites

The hardness values for sintered Ti6Al4V reinforced with TiN-TiB_2 vol.% are shown in Fig. 6. The hardness of Ti6Al4V with no reinforcement has the lowest hardness value of 378 $HV_{0.2}$. Nevertheless, the inclusion of ceramic particles enhances the hardness to 707 $HV_{0.2}$, which has the highest hardness value. The addition of ceramic particles to the Ti6Al4V matrix increases hardness. This might be attributed to uniformly distributed reinforcement or the creation of new hard phases (TiB and Ti_2N) in the Ti6Al4V matrix, which reduces particle spacing and restricts dislocation movement (Ref 38, 41, 42). Several factors contributed to this increase in hardness, including grain size, composition, decreased porosity, grain refinement, and the dispersion hardening effect produced by the titanium matrix reinforcing phases (Ref 36). However, reinforcing ceramic-particles reduce the energy at the grain boundary and weaken movability, which further blocks the dislocation movement. This barrier stabilizes the grains by limiting grain growth at a high temperature, allowing them to remain stable and increasing their hardness (Ref 43, 44).

3.4 Wear Behavior of Sintered Titanium Matrix Composites

The frictional coefficient is critical for determining the heat generated by friction between the counterface material and the specimen surface (Ref 45, 46). Figure 7a depicts the trend for the Ti6Al4V alloy and composites. The coefficient of friction ranges between 0.3 and 0.65, as seen in the plot, and decreases slightly as a ceramic substance is introduced. This demonstrates that the reinforcement particles impede the counterface balls' easy gliding across the specimen's surface, reducing the heat generated. The composite sintered with 5 vol.% TiB_2 has the highest wear resistance and is more resistant to abrasion and plastic deformation. This might be owing to the material's extreme hardness and density. However, the composite containing 5% TiN exhibits a considerable degree of instability in the early phases, before attaining a steady state toward the end. The initial instability might be attributed to the running-in period and unstable surface roughness between the specimen surface and the counterface material (Ref 47, 48). This behavior might be related to the polishing procedure employed during

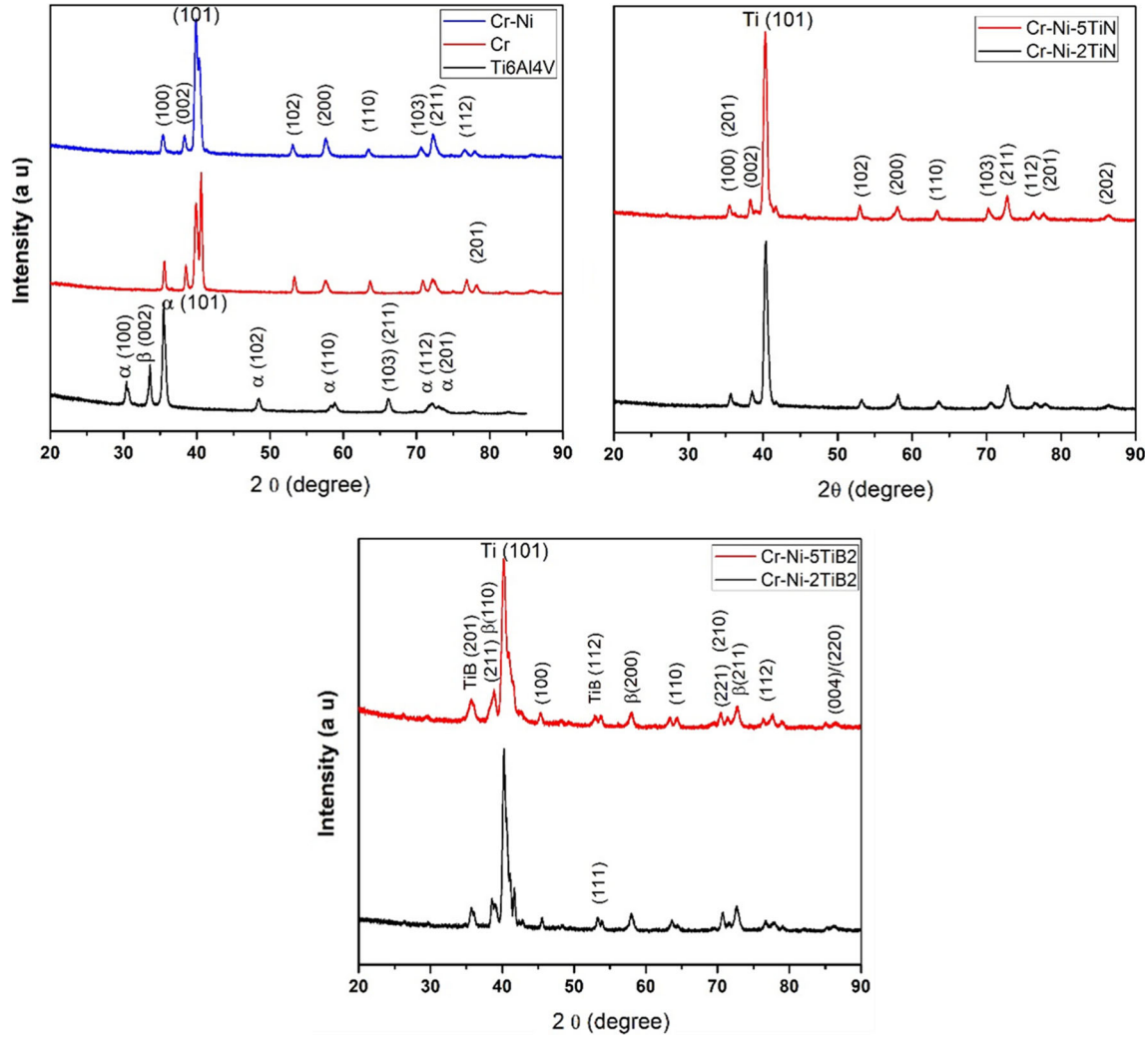

Fig. 5 X-ray diffraction pattern of Ti6Al4V-Ni-Cr reinforced TiN-TiB_2

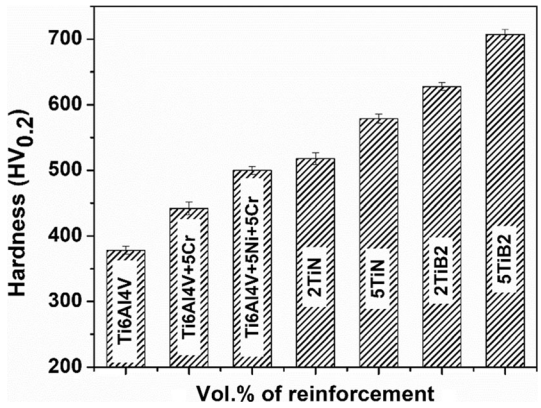

Fig. 6 Hardness value of sintered titanium matrix composite

the sliding wear test, which aimed to generate a smooth wear surface by removing surface roughness or the imperfections imposed by the nitride and boride reinforcing particles (Ref 49). The coefficient of friction values fluctuated due to the continual building and breaking of the friction-reducing layer generated by the mechanical action of the counterface material. Another factor to consider is the existence of hybrid reinforcements, which can increase the hardness and strength of the composite while also establishing strong interfacial bonding between the matrix and the reinforcement particles. The observed significant difference between the frictional coefficient of the reinforced and unreinforced Ti6Al4V alloys can be attributed to two different mechanisms: plastic deformation in the softer matrix and the easy formation of debris along the wear track, which in turn promotes heat generation (Ref 36). It is also worth noting that the sintered titanium-based composite frictional coefficient decreases. This might be due to potential later oxide formation, which acts as a lubricant reducing friction between the two gliding surfaces. Figure 7b, c illustrates the wear volume and rate under a 10 N applied load. The wear volume and wear rate values reduced steadily as the reinforcing phase increased. This prevented plastic deformation and ensured the retention of the relative surface smoothness of the titanium-based composite during dry sliding wear. These phenomena might be connected to the distribution of microhardness. Furthermore, increased hardness due to the formation of hard phases (Ti_2N and TiB) with some unreacted TiB reinforcement has a significant influence on the hardness, making the material more wear resistant (Ref 50, 51).

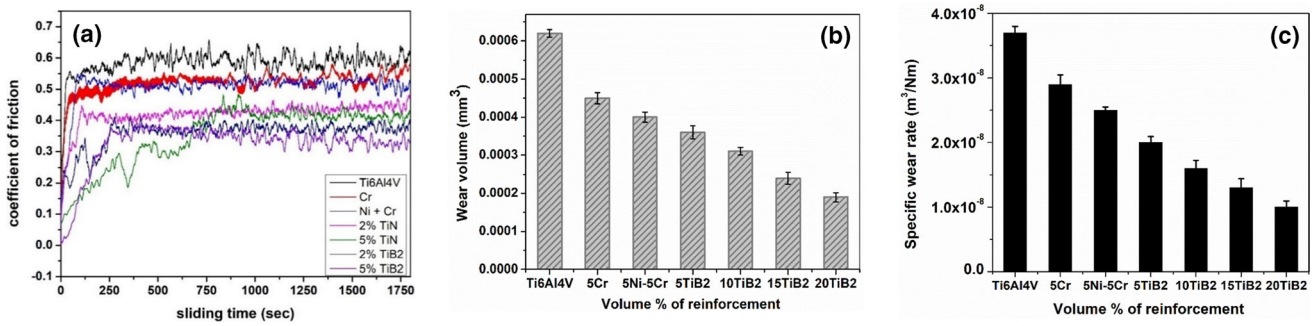

Fig. 7 Wear behavior of sintered titanium matrix composite material under a load of 10 N: **a** coefficient of friction, **b** wear volume and **c** specific wear rate

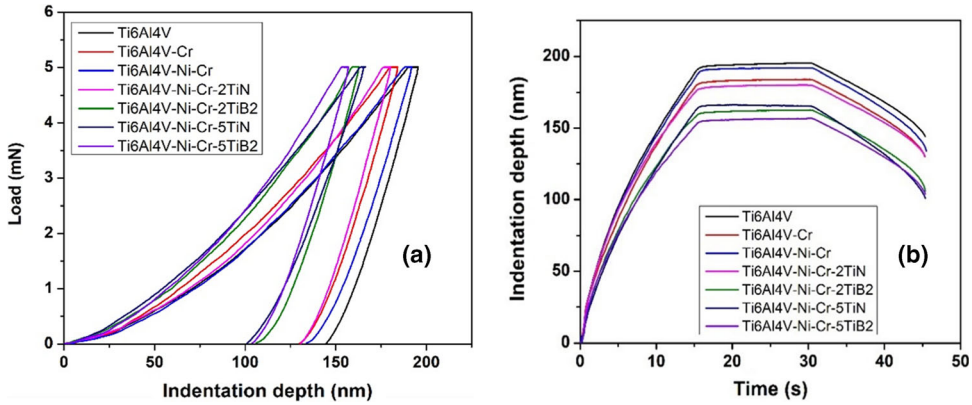

Fig. 8 Plots of **a** Load against displacement and **b** indentation depth against time for sintered titanium matrix composites

3.5 Nanoindentation Studies of the Sintered Titanium Matrix Composites

The load-displacement curves of the sintered titanium matrix composite are depicted in Fig. 8a. According to the indentation curves, the sintered titanium matrix composite demonstrated successive loading and unloading behaviors under the influence of the load applied. Nevertheless, the elastic-plastic deformation behavior differed owing to the presence of the dispersed reinforcement particles. Ti6Al4V had the most significant penetration depth, followed by Ti6Al4V-5Ni-5Cr, Ti6Al4V-5Ni-5Cr-2TiN, Ti6Al4V-5Ni-5Cr-2TiB_2, Ti6Al4V-5Ni-5Cr-5TiN, and Ti6Al4V-5Ni-5Cr-5TiB_2. This indicates that adding ceramics (TiN/TiB_2) improved the titanium matrix composites' resistance to plastic deformation during indentation. This implies an improvement in hardness and stiffness due to load transfer from the matrix to the reinforcement (Ref 25). The curve shows the impact of the chromium-based reinforcements, the prevention of a deep penetration of the indenter surface into the specimen. This implies that the reinforced Ti6Al4V alloys are more resistant to plastic deformation. The strengthening mechanism exhibited by the reinforced Ti6Al4V alloys can also be attributed to the lattice distortion and BCC strengthening phase formed by the reinforcement particles. Li et al. reported a similar observation in a recent study (Ref 52). Furthermore, the produced BCC phase minimizes sliding planes, inhibits interplanar dislocations, resists plastic deformation, and causes microstructural stabilization (Ref 53). Figure 8b shows the indentation depth against the time of the sintered titanium matrix composite. The Ti6Al4V alloy exhibited significant plastic deformation, with a maximum indentation depth of 195.26 nm. With the addition of reinforcements, penetration decreased from 192.54 to 157.92 nm. However, the reduced penetration depth indicates plastic deformability with the addition of the respective reinforcements (Ref 54). The best resistance to indentation loads with penetration depth is Ti6Al4V-5Ni-5Cr-5TiB_2. According to these studies, combining Ni-Cr with ceramics enhanced the hardness and stiffness of titanium matrix composites. The increase in mechanical properties may be attributed to the load transfer mechanism, from the matrix to the reinforcement, caused by the pinning effect of the dislocation motion engendered by the ceramics in the titanium matrix composite.

Table 2 shows the hardness (H) and reduced elastic modulus (Er) of the titanium matrix composite produced by nanoindentation. It must be noted that the nanohardness follows the same trend as the reduced elastic modulus. The incorporation of TiN-TiB_2 enhances hardness and reduces elastic modulus values, with Ti6Al4V-Ni-Cr-5TiB_2 having the maximum nanohardness of 10.343 GPa and an elastic modulus of 158.93 GPa. The improved hardness and elastic modulus of Ti6Al4V matrix composites can be caused by a decreased β phase within the composite. As a result, the TiN and TiB_2 reinforcements are assumed to have served as stabilizers, increasing the proportion of α martensitic phase in the Ti6Al4V composite. An increase in stabilizer content promotes a martensitic transformation (β to α), thereby increasing the volume fraction of the α phase (Ref 26). Previous research has demonstrated that the β phase with BCC crystalline structure often exhibits reduced hardness and elastic modulus, compared to the orthorhombic α phase (Ref

Table 2 Nanoindentation values *of sintered titanium matrix composite, including hardness (H), modulus of elasticity, maximum depth, and contact depth*

Samples	Hardness (HIT) MPa	Micro-hardness HVIT	Mod. of elasticity (EIT) GPa	Max. depth, nm	Contact depth, nm
Ti6Al4V	6363.3	589.31	131.58	195.26	166.98
Ti6Al4V + 5Cr	6898.9	638.92	125.27	192.54	159.55
Ti6Al4V + 5Ni + 5Cr	6791.1	628.93	125.52	191.98	161.02
Ti6Al4V + 5Ni + 5Cr + 2TiN	7765.9	719.2	142.88	180.51	149.32
Ti6Al4V + 5Ni + 5Cr + 2TiB_2	9352.8	866.17	164.05	162.96	134.76
Ti6Al4V + 5 Ni + 5Cr + 5TiN	10,070	932.57	159.89	165.88	126.32
Ti6Al4V + 5Ni + 5Cr + 5TiB_2	10,343	957.85	167.9	157.29	127.43

Table 3 Nanoindentation *of sintered titanium matrix composite*, including elastic modulus, H/E_r, H^3/E_r^2

Samples	Elastic modulus, (E_r) GPa	H/E_r	H^3/E_r^2, GPa
Ti6Al4V	128.4	0.0495	0.0156
Ti6Al4V + 5Cr	122.9	0.0561	0.0217
Ti6Al4V + 5Ni + 5Cr	123.12	0.0551	0.0206
Ti6Al4V + 5Ni + 5Cr + 2TiN	138.1	0.0562	0.0245
Ti6Al4V + 5Ni + Cr + 2TiB_2	155.78	0.0600	0.0337
Ti6Al4V + 5Ni + 5Cr + 5TiN	157.02	0.0641	0.0414
Ti6Al4V + 5Ni + 5Cr + 5TiB_2	158.93	0.0650	0.0438

55, 56). Therefore, a high concentration of the β phase reduces hardness and elastic modulus. These results further indicate that incorporating the reinforcement particles into the Ti6Al4V particles enhances the nanomechanical properties of the alloy by preventing free dislocation movement in the composites. The strength of a material is proportional to its hardness; and a harder substance is stronger (Ref 57). The H^3/Er^2 is a valuable means of defining a material's capacity to resist plastic deformation under loaded contact, resulting in superior wear (Ref 58). The increase in H^3/Er^2 relative to the unreinforced Ti6Al4V alloy, as shown in Table 3, indicates that Ti6Al4V composites have better wear resistance. This makes them good alternatives in applications requiring advanced materials with high wear resistance.

4. Conclusions

This study utilized spark plasma sintering to examine the impact of TiN-TiB_2 on the densification, microstructure, hardness, phase change, and wear behavior of the Ti6Al4V-Ni-Cr matrix. The conclusions are as follows:

1. Ti6Al4V-Ni-Cr composites with TiN-TiB_2 achieve a complete densification ranging from 99.51 to 95.33%.
2. The reinforcement phase was distributed evenly; and the microstructural transformation confirms the presence of lamellar (α and β phase) and bimodal structures in titanium matrix composites.
3. The average microhardness value grew steadily from 378 to 707 $HV_{0.2}$ upon incorporating the TiN-TiB_2 content.
4. The steady-state friction coefficient of the Ti6Al4V-Ni-Cr matrix composite ranges between 0.3 and 0.65. This demonstrates that incorporating ceramic particles enhances the wear resistance of the composite. The sintered composite frictional coefficient may be attributed to delayed oxide development, which serves as a lubricant and minimizes friction between the two gliding surfaces.
5. The addition of TiN-TiB_2 increased hardness from 6363.3 to 10,343 MPa, and elastic modulus from 128.4 to 158.93 GPa. Ti6Al4V + 5Ni + 5Cr + 5TiB_2 had the most excellent elastic modulus (Er) and hardness (H). The increased hardness and reduced elastic modulus of Ti6Al4V-Ni-Cr matrix composites can be attributed to the reduced β phase within the composite.

Authors Contributions

OEF conceptualization, research laboratory works, data validation, report writing. SRO laboratory work, report writing and discussion of data. SOA research laboratory work, report writing, data validation. OOA research laboratory work, report writing. AOA laboratory work, report writing. SGB research laboratory work. AAA report writing, review. PAO review, data validation and laboratory funding support.

Funding Statement

No funds, grants, or other support was received.

Availability of data and materials

Data will be made available on request.

Competing interests

The authors have no conflicts of interest to declare relevant to this article's content.

Ethical Approval

The submitted work is original and has never been published in any form or language.

Consent to Participate

All authors agreed and participated in the production of the manuscript.

Consent for Publication

The authors have all agreed to submit the work for consideration and publication for peer review in this journal.

References

1. V.S. Balaji and S. Kumaran, Densification and Microstructural Studies of Titanium-Boron Carbide (B4C) Powder Mixture during Spark Plasma Sintering, *Powder Technol.*, 2014, **264**, p 536-540.
2. A.S. Namini, M. Azadbeh and M.S. Asl, Effect of TiB2 Content on the Characteristics of Spark Plasma Sintered Ti-TiBw Composites, *Adv. Powder Technol.*, 2017, **28**(6), p 1564-1572.
3. Z. Ahmadi, M.S. Asl, M. Zakeri, and M. Farvizi, Fabrication of (Zr, Ti) B2-ZrN-BN Composites through Reactive Spark Plasma Sintering of ZrB2 and TiN, *Micron*, 2021, p 103203
4. A. Purwar, R. Mukherjee, K. Ravikumar, S. Ariharan, N.K. Gopinath and B. Basu, Development of ZrB2-SiC-Ti by Multi Stage Spark Plasma Sintering at 1600° C, *J. Ceram. Soc. Jpn.*, 2016, **124**(4), p 393-402.
5. L.L. Dong, W. Zhang, Y.Q. Fu, J.W. Lu, Y. Liu and Y.S. Zhang, Synergetic Enhancement of Strength and Ductility for Titanium-Based Composites Reinforced with Nickel Metallized Multi-Walled Carbon Nanotubes, *Carbon*, 2021, **184**, p 583-595.
6. K.B. Panda and K.S.R. Chandran, Synthesis of Ductile Titanium-Titanium Boride (Ti-TiB) Composites with a Beta-Titanium Matrix: The Nature of TiB Formation and Composite Properties, *Metall. Mater. Trans. A.*, 2003, **34**(6), p 1371-1385.
7. R.W. Schutz, Environmental Behavior of Beta Titanium Alloys, *JOM*, 1994, **46**(7), p 24-29.
8. G.B. Raju, A. Mukhopadhyay, K. Biswas and B. Basu, Densification and High-Temperature Mechanical Properties of Hot Pressed TiB2-(0-10 wt%) MoSi2 Composites, *Scripta Mater.*, 2009, **61**(7), p 674-677.
9. C. Subramanian, T.S.R.C. Murthy and A.K. Suri, Synthesis and Consolidation of Titanium Diboride, *Int. J. Refract Metal Hard Mater.*, 2007, **25**(4), p 345-350.
10. P.H.C. Camargo, K.G. Satyanarayana and F. Wypych, Nanocomposites: Synthesis, Structure, Properties and New Application Opportunities, *Mater. Res.*, 2009, **12**(1), p 1-39.
11. M.E. Maja, O.E. Falodun, B.A. Obadele, S.R. Oke, and P.A. Olubambi, Nanoindentation Studies on TiN Nanoceramic Reinforced Ti-6Al-4V Matrix Composite, *Ceramics International*, 2018, **44**(4)
12. Y. Zheng, S. Wang, Y. Yan, N. Zhao and X. Chen, Microstructure Evolution and Phase Transformation during Spark Plasma Sintering of Ti (C, N)-Based Cermets, *Int. J. Refract Metal Hard Mater.*, 2008, **26**(4), p 306-311.
13. T. Venkateswaran, B. Basu, G.B. Raju and D.-Y. Kim, Densification and Properties of Transition Metal Borides-Based Cermets via Spark Plasma Sintering, *J. Eur. Ceram. Soc.*, 2006, **26**(13), p 2431-2440.
14. O.E. Falodun, B.A. Obadele, S.R. Oke, O.O. Ige, P.A. Olubambi, M.L. Lethabane, and S.W. Bhero, Influence of Spark Plasma Sintering on Microstructure and Wear Behaviour of Ti-6Al-4V Reinforced with Nanosized TiN, *Trans. Nonferrous Metals Soc. China (English Edition)*, 2018, **28**(1)
15. M. Tokita, Progress of Spark Plasma Sintering (SPS) Method, Systems, Ceramics Applications and Industrialization, *Ceramics*, 2021, **4**(2), p 160-198.
16. N. Saheb, Z. Iqbal, A. Khalil, A.S. Hakeem, N. Al Aqeeli, T. Laoui, A. Al-Qutub, and R. Kirchner, Spark Plasma Sintering of Metals and Metal Matrix Nanocomposites: A Review, *J. Nanomater*, 2012, **2012**
17. O.E. Falodun, B.A. Obadele, S.R. Oke, A.M. Okoro and P.A. Olubambi, Titanium-Based Matrix Composites Reinforced with ParticulateM, Microstructure, and Mechanical Properties Using Spark Plasma Sintering Technique: A Review, *Int. J. Adv. Manufact. Technol.*, 2019, **102**(5-8), p 1689-1701.
18. B.A. Obadele, O.E. Falodun, S.R. Oke, and P.A. Olubambi, Spark Plasma Sintering Behaviour of Commercially Pure Titanium Micro-Alloyed with Ta-Ru, *Partic. Sci. Technol.* 2019, **37**(7)
19. Y.H. Wang, J.P. Lin, Y.H. He, Y.L. Wang, and G.L. Chen, Fabrication and SPS Microstructures of Ti-45Al-8.5 Nb-(W, B, Y) Alloying Powders, *Intermetallics*, 2008, **16**(2), p 215-224
20. O.O. Ige, S.R. Oke, O.E. Falodun, S. Aribo, K.M. Oluwasegun, O.O. Ajibola, J.O. Olawale, A. Ogunbadejo, O.T. Olalemi, and P.A. Olubambi, Effect of Flow Velocity on Corrosion Behaviour of Spark Plasma Sintered Fe-Cr-Ni Reinforced with TiN in 3.5 Wt% NaCl, *Mater. Today Proc.* 2020
21. A. Couret, G. Molénat, J. Galy and M. Thomas, Microstructures and Mechanical Properties of TiAl Alloys Consolidated by Spark Plasma Sintering, *Intermetallics*, 2008, **16**(9), p 1134-1141.
22. H. Feng, Y. Zhou, D. Jia and Q. Meng, Rapid Synthesis of Ti Alloy with B Addition by Spark Plasma Sintering, *Mater. Sci. Eng., A*, 2005, **390**(1-2), p 344-349.
23. A.M. Okoro, S.S. Lephuthing, M.A. Awotunde, O.E. Falodun, R. Machaka and P.A. Olubambi, Nanomechanical Properties of Spark Plasma Sintered Multiwall Carbon Nanotubes Reinforced Ti6Al4V Nanocomposites via Nanoindentation Technique, *Mater. Today: Proc.*, 2020, **28**, p 717-720.
24. H. Attar, S. Ehtemam-Haghighi, D. Kent, I.V. Okulov, H. Wendrock, M. Bönisch, A.S. Volegov, M. Calin, J. Eckert and M.S. Dargusch, Nanoindentation and Wear Properties of Ti and Ti-TiB Composite Materials Produced by Selective Laser Melting, *Mater. Sci. Eng., A*, 2017, **688**, p 20-26.
25. A.M. Okoro, R. Machaka, S.S. Lephuthing, S.R. Oke, M.A. Awotunde and P.A. Olubambi, Nanoindentation Studies of the Mechanical Behaviours of Spark Plasma Sintered Multiwall Carbon Nanotubes Reinforced Ti6Al4V Nanocomposites, *Mater. Sci. Eng., A*, 2019, **765**, 138320.
26. S. Ehtemam-Haghighi, G. Cao and L.-C. Zhang, Nanoindentation Study of Mechanical Properties of Ti Based Alloys with Fe and Ta Additions, *J. Alloy. Compd.*, 2017, **692**, p 892-897.
27. G.R. Baran, The Metallurgy of Ni-Cr Alloys for Fixed Prosthodontics, *J. Prosthet. Dent.*, 1983, **50**(5), p 639-650.
28. F. Faot, W.J. da Silva, R.C.M.R. Garcia and A.A.D.B. Cury, Microstructural Characterization of Ni-Cr-Mo-Ti and Ti-6Al-4V Alloys Used in Prosthetic Abutments, *Revista Odonto Ciência*, 2009, **24**(4), p 401-405.
29. O.E. Falodun, S.R. Oke, B.A. Obadele, A.M. Okoro and P.A. Olubambi, Influence of SiAlON Ceramic Reinforcement on Ti6Al4V Alloy Matrix via Spark Plasma Sintering Technique, *Met. Mater. Int.*, 2021, **27**(6), p 1769-1778.
30. S.R. Oke, O.O. Ige, O.E. Falodun, B.A. Obadele, M.B. Shongwe and P.A. Olubambi, Optimization of Process Parameters for Spark Plasma Sintering of Nano Structured SAF 2205 Composite, *J. Market. Res.*, 2018, **7**(2), p 126-134.
31. A. Teber, F. Schoenstein, F. Têtard, M. Abdellaoui and N. Jouini, Effect of SPS Process Sintering on the Microstructure and Mechanical Properties of Nanocrystalline TiC for Tools Application, *Int. J. Refract Metal Hard Mater.*, 2012, **30**(1), p 64-70.
32. F.M. Kgoete, A.P.I. Popoola and O.S.I. Fayomi, Influence of Spark Plasma Sintering on Microstructure and Corrosion Behaviour of Ti-6Al-4V Alloy Reinforced with Micron-Sized Si3N4 Powder, *Defence Technology*, 2018, **14**(5), p 403-407.
33. A.M. Locci, R. Orru, G. Cao and Z.A. Munir, Effect of Ball Milling on Simultaneous Spark Plasma Synthesis and Densification of TiC-TiB2 Composites, *Mater. Sci. Eng., A*, 2006, **434**(1-2), p 23-29.
34. O.E. Falodun, B.A. Obadele, S.R. Oke, M.E. Maja, and P.A. Olubambi, Effect of Sintering Parameters on Densification and Microstructural Evolution of Nano-Sized Titanium Nitride Reinforced Titanium Alloys, *J. Alloys Compd.* 2018, **736**
35. S.A. Delbari, A.S. Namini and M.S. Asl, Hybrid Ti Matrix Composites with TiB2 and TiC Compounds, *Mater. Today Commun.*, 2019, **20**, 100576.

36. A.S. Namini, S.A.A. Dilawary, A. Motallebzadeh and M.S. Asl, Effect of TiB2 Addition on the Elevated Temperature Tribological Behavior of Spark Plasma Sintered Ti Matrix Composite, *Compos. B Eng.*, 2019, **172**, p 271-280.
37. J.O. Abe, A.P.I. Popoola and O.M. Popoola, Consolidation of Ti6Al4V Alloy and Refractory Nitride Nanoparticles by Spark Plasma Sintering Method: Microstructure Mechanical, Corrosion and Oxidation Characteristics, *Mater. Sci. Eng., A*, 2020, **774**, 138920.
38. O.E. Falodun, B.A. Obadele, S.R. Oke, O.O. Ige and P.A. Olubambi, Effect of TiN and TiCN Additions on Spark Plasma Sintered Ti-6Al-4V, *Part. Sci. Technol.*, 2020, **38**(2), p 156-165.
39. M. Esmaily, S.N. Mortazavi, P. Todehfalah and M. Rashidi, Microstructural Characterization and Formation of A′ Martensite Phase in Ti-6Al-4V Alloy Butt Joints Produced by Friction Stir and Gas Tungsten Arc Welding Processes, *Mater. Des.*, 2013, **47**, p 143-150.
40. A. Amanov, B. Urmanov, T. Amanov and Y.S. Pyun, Strengthening of Ti-6Al-4V Alloy by High Temperature Ultrasonic Nanocrystal Surface Modification Technique, *Mater. Lett.*, 2017, **196**, p 198-201.
41. K.K. Alaneme, O.P. Adu, S.R. Oke, O.E. Falodun, and P.A. Olubambi, Densification Characteristics, Microstructure and Wear Behaviour of Spark Plasma Sintering Processed Titanium-Niobium Pentoxide (Ti-Nb<inf>2</Inf>O<inf>5</Inf>) Based Composites, *J. King Saud Univ. Eng. Sci.* 2020
42. O.E. Falodun, S.R. Oke, B.A. Obadele, A.M. Okoro, and P.A. Olubambi, Influence of SiAlON Ceramic Reinforcement on Ti6Al4V Alloy Matrix via Spark Plasma Sintering Technique, *Metals Mater. Int.* 2019, p 1-10
43. B. Stalin, M. Ravichandran, G.T. Sudha, A. Karthick, K.S. Prakash, A.B. Asirdason and S. Saravanan, Effect of Titanium Diboride Ceramic Particles on Mechanical and Wear Behaviour of Cu-10 Wt% W Alloy Composites Processed by P/M Route, *Vacuum*, 2021, **184**, 109895.
44. J. Ďurišin, K. Ďurišinová, M. Orolínová and K. Saksl, Effect of the MgO Particles on the Nanocrystalline Copper Grain Stability, *Mater. Lett.*, 2004, **58**(29), p 3796-3801.
45. S.O. Akinwamide, S.M. Lemika, B.A. Obadele, O.J. Akinribide, B.T. Abe and P.A. Olubambi, Characterization and Mechanical Response of Novel Al-(Mg-TiFe-SiC) Metal Matrix Composites Developed by Stir Casting Technique, *J. Compos. Mater.*, 2019, **53**(28-30), p 3929-3938.
46. S.O. Akinwamide, S.M. Lemika and B. Abiodun, Study of Microstructural and Mechanical Properties of Stir Cast Al (SiC-Mg-TiFe) Composite, *Fluid Dyn. Mater. Proc.*, 2019, **15**(1), p 15-26.
47. D. Gu, Y.-C. Hagedorn, W. Meiners, K. Wissenbach and R. Poprawe, Nanocrystalline TiC Reinforced Ti Matrix Bulk-Form Nanocomposites by Selective Laser Melting (SLM): Densification, Growth Mechanism and Wear Behavior, *Compos. Sci. Technol.*, 2011, **71**(13), p 1612-1620.
48. N. Tian, L.L. Dong, H.L. Wang, Y.Q. Fu, W.T. Huo, Y. Liu, J.S. Yu and Y.S. Zhang, Microstructure and Tribological Properties of Titanium Matrix Nanocomposites through Powder Metallurgy Using Graphene Oxide Nanosheets Enhanced Copper Powders and Spark Plasma Sintering, *J. Alloy. Compd.*, 2021, **867**, 159093.
49. S.R. Oke, O.O. Ige, O.E. Falodun, B.A. Obadele, M.R. Mphahlele, and P.A. Olubambi, Influence of Sintering Process Parameters on Corrosion and Wear Behaviour of SAF 2205 Reinforced with Nano-Sized TiN, *Mater. Chem. Phys.* 2018, **206**
50. A. Sabahi Namini, M. Azadbeh, and M. Shahedi Asl, Effects of In-Situ Formed TiB Whiskers on Microstructure and Mechanical Properties of Spark Plasma Sintered Ti-B4C and Ti-TiB2 Composites, *Scientia Iranica*, 2018, **25**(2), p 762-771
51. L.J. Huang, L. Geng, B. Wang and L.Z. Wu, Effects of Volume Fraction on the Microstructure and Tensile Properties of in Situ TiBw/Ti6Al4V Composites with Novel Network Microstructure, *Mater. Des.*, 2013, **45**, p 532-538.
52. J. Li, Q. Fang, B. Liu, Y. Liu and Y. Liu, Atomic-Scale Analysis of Nanoindentation Behavior of High-Entropy Alloy, *J. Micromech Mol. Phys.*, 2016, **1**(01), p 1650001.
53. G.N. Mekgwe, O.J. Akinribide, S.O. Akinwamide and P.A. Olubambi, Fabrication of Graphite Reinforced TiCxNy by Spark Plasma Sintering Technique: A Comparative Assessment of Microstructural Integrity and Nanoindentation Properties, *Vacuum*, 2021, **187**, 110144.
54. S.O. Akinwamide, O.J. Akinribide and P.A. Olubambi, Microstructural Evolution, Mechanical and Nanoindentation Studies of Stir Cast Binary and Ternary Aluminium Based Composites, *J. Alloy. Compd.*, 2021, **850**, 156586.
55. A.C.L. Faria, R.C.S. Rodrigues, A.P.R.A. Claro, M. da G.C. de Mattos, and R.F. Ribeiro, Wear Resistance of Experimental Titanium Alloys for Dental Applications. *J. Mech. Behav. Biomed. Mater.* 2011, **4**(8), p 1873-1879
56. S. Ehtemam-Haghighi, Y. Liu, G. Cao and L.-C. Zhang, Influence of Nb on the B $\rightarrow$ α''martensitic Phase Transformation and Properties of the Newly Designed Ti-Fe-Nb Alloys, *Mater. Sci. Eng., C*, 2016, **60**, p 503-510.
57. P. Zhang, S.X. Li and Z.F. Zhang, General Relationship between Strength and Hardness, *Mater. Sci. Eng., A*, 2011, **529**, p 62-73.
58. J. Musil, F. Kunc, H. Zeman and H. Polakova, Relationships between Hardness, Young's Modulus and Elastic Recovery in Hard Nanocomposite Coatings, *Surf. Coat. Technol.*, 2002, **154**(2-3), p 304-313.